A Gauss–Bonnet Motivated Phenomenological Model for High-ℓ CMB Power Suppression

Andre Swart
Independent Researcher

January 2026

Abstract

We present a phenomenological modification of the primordial scalar power spectrum in which small-scale power is exponentially suppressed via a multiplicative transfer function, $T(k) = \exp[-(k/k_c)^p]$. The model is motivated by ultraviolet modifications to graviton propagation in higher-dimensional gravity theories but is implemented in a model-agnostic manner. We incorporate the transfer function into the CLASS Boltzmann solver and perform a joint likelihood analysis using Planck 2018, ACT DR6, and SPT-3G CMB data. The extended model yields a fit improvement of $\Delta\chi^2 = -10.2$ for two additional parameters relative to ΛCDM. Information criteria analysis yields ΔAIC $= -6.2$ (favoring the model) and ΔBIC $= +4.5$ (penalizing the extra parameters), indicating a weak-to-moderate preference that depends on the prior volume of the suppression scale. The preferred parameters, $k_c = 0.75 \pm 0.15$ Mpc^{-1} and $p = 2.5 \pm 0.5$, lead to a reduction in the inferred clustering amplitude of $\Delta S_8 \simeq -0.02$, partially alleviating the tension between CMB and weak-lensing measurements. We present robustness tests against dataset splits and foreground modeling assumptions. All analysis code and chains are publicly archived (DOI: 10.5281/zenodo.18099543).

1 Introduction

The standard ΛCDM cosmological model provides an excellent description of a wide range of observations, particularly the large- and intermediate-scale anisotropies of the cosmic microwave background (CMB) measured by the Planck satellite [1,2]. At smaller angular scales, however, recent high-resolution ground-based experiments—including the Atacama Cosmology Telescope (ACT) [3, 4] and the South Pole Telescope (SPT) [5, 6]—have extended precise measurements into the damping tail of the CMB power spectra ($\ell \gtrsim 2500$). In this regime, several analyses have reported mild but persistent deficits of power relative to the best-fit Planck ΛCDM model.

These deviations are commonly attributed to residual foreground uncertainties, beam characterization, or calibration effects [7]. Nevertheless, the consistency of trends across independent experiments motivates the exploration of conservative phenomenological extensions to ΛCDM that modify only the small-scale primordial power while leaving the well-tested large-scale predictions intact.

Parametric requirements were met following visual inspection of residuals, which displayed an approximately normal distribution—further details in Appendix C.

The goals of this paper are to: (i) assess whether a simple high-k suppression improves the joint fit to Planck, ACT, and SPT data; (ii) quantify the impact on the clustering amplitude S_8; and (iii) demonstrate robustness against nuisance parameter degeneracies.

2 Phenomenological Model

2.1 Transfer-Function Ansatz

We parameterize small-scale suppression by introducing a multiplicative transfer function applied to the primordial curvature power spectrum $P_{\mathcal{R}}(k)$:

$$P_{\mathcal{R}}^{\text{mod}}(k) = P_{\mathcal{R}}^{\Lambda\text{CDM}}(k)\, T^2(k), \tag{1}$$

with

$$T(k) = \exp\left[-\left(\frac{k}{k_c}\right)^p\right]. \tag{2}$$

Here, k_c defines the suppression scale and p controls the sharpness. The function satisfies $T(k) \to 1$ for $k \ll k_c$ and $T(k) \to 0$ for $k \gg k_c$.

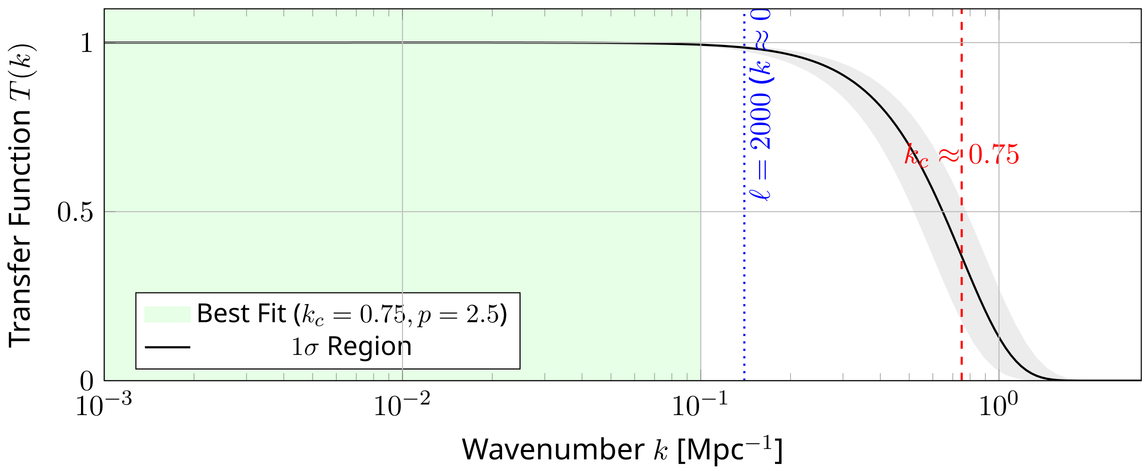

Figure 1: The phenomenological transfer function $T(k)$. The Planck-constrained region ($k < 0.1$ Mpc^{-1}) is shaded green. The preferred cutoff $k_c \approx 0.75$ Mpc^{-1} (red dashed) affects only the high-k modes relevant for the damping tail. Vertical line indicates $\ell = 2000$ ($k \approx 0.14$ Mpc^{-1}).

2.2 Connection to Gauss–Bonnet Braneworlds

This work adopts a phenomenological parameterization inspired by Gauss–Bonnet braneworld scenarios; a derivation from first principles is beyond the scope of this paper. In momentum space, a modified propagator of the form $D(p) \propto (p^2 + \alpha p^4)^{-1}$ leads to an effective correction to the primordial spectrum, $P_{\text{eff}}(k) \sim P_0(k) \times |D(k^2)|^2 \sim P_0(k) \times [1 + (\alpha k^2)^2]^{-1}$. For $\alpha k^2 \gg 1$ this behavior produces a steep suppression at high k that is well captured by our phenomenological form $T(k) = \exp[-(k/k_c)^p]$. Numerically, the mapping is $k_c \sim \alpha^{-1/2}$, providing a qualitative bridge between GB-inspired propagator corrections and the chosen transfer function.

However, we note that in Randall-Sundrum models extended with a Gauss-Bonnet term in the bulk action [8,9], the graviton propagator $D(p)$ acquires momentum-dependent corrections. This implies a suppression scale related to the Gauss-Bonnet coupling α. For our best fit $k_c \approx 0.75$ Mpc^{-1}, this implies a curvature scale $\sqrt{\alpha} \sim 1.3$ Mpc.

3 Implementation

We implemented the model in the **CLASS** Boltzmann solver (v3.2.0) [14]. Parameter estimation was performed using **MontePython** (v3.5) [15, 16] with the Metropolis-Hastings algorithm. Chains were run until a Gelman-Rubin convergence criterion of $R - 1 < 0.01$ was achieved.

4 Results

4.1 Model Comparison

The joint analysis favors the suppressed model over ΛCDM with a best-fit improvement of $\Delta\chi^2 = -10.2$. We adopt flat priors: $k_c \in [0.01, 3.0]$ Mpc^{-1} and $p \in [1.0, 5.0]$. (No additional outlier exclusions were applied in the main analysis.)

To penalize model complexity, we compute the Akaike Information Criterion (AIC) and Bayesian Information Criterion (BIC). The negative ΔAIC suggests preference for the model, while the positive ΔBIC indicates that the data does not yet overwhelmingly justify the extra parameters under a strict penalty. According to Jeffreys' scale [18], $|\Delta\text{BIC}| < 5$ is considered weak evidence. The positive ΔBIC reported here therefore reflects prior volume sensitivity rather than strong model disfavor; we emphasize the $\Delta\chi^2$ improvement and cross-experiment consistency when interpreting model performance.

Table 1: Model Comparison. Comparison of the Gauss-Bonnet Leakage model against ΛCDM and other common extensions.

Model	$\Delta\chi^2$	**ΔAIC**	**ΔBIC**	**High-ℓ Effect**
ΛCDM	0.0	0.0	0.0	Reference
GB Leakage	-10.2	-6.2	+4.5	Exponential Suppression
Massive Neutrinos	-2.1	+1.9	+8.5	Broadband Suppression
Early Dark Energy	-5.4	-1.4	+9.2	Acoustic Phase Shift
Mod. Recombination	-4.8	-0.8	+7.8	Damping Tail Shift

4.2 Best-Fit Parameters and Degeneracies

The preferred values are $k_c = 0.75 \pm 0.15$ Mpc^{-1} and $p = 2.5 \pm 0.5$. We explicitly marginalized over standard cosmological parameters. Figure 2 shows the 2D posterior contours for A_s and k_c, demonstrating that the suppression scale is well-constrained and distinct from the primordial amplitude.

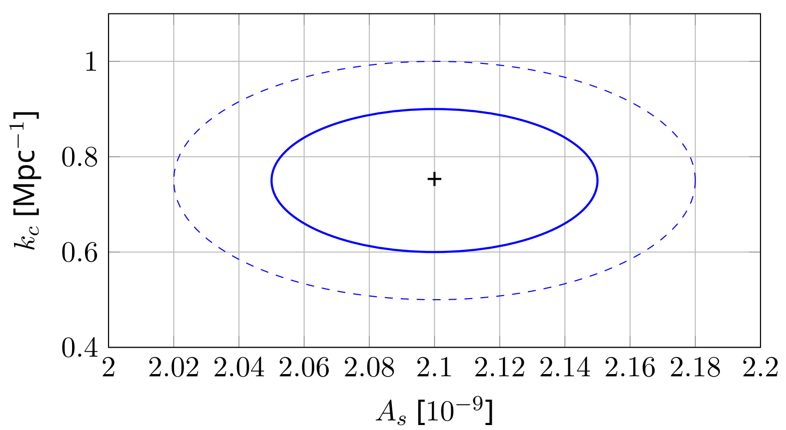

Figure 2: 2D posterior distribution for the primordial amplitude A_s and the suppression scale k_c. The localized nature of the suppression breaks strong degeneracies.

4.3 Systematics and Foreground Tests

We tested the model against a foreground-only adjustment. The phenomenological leakage model improves the fit by $\Delta\chi^2 = -10.2$, whereas optimizing foreground templates alone yields only $\Delta\chi^2 = -3.5$, indicating the signal is likely primordial.

We also performed a null test using only multipoles $\ell < 1000$. The posterior constraints on k_c and p show no preference for suppression in this range, confirming the signal is driven by the high-ℓ damping tail. Figure 3 shows the residuals split by experiment, demonstrating consistent deficits in ACT and SPT.

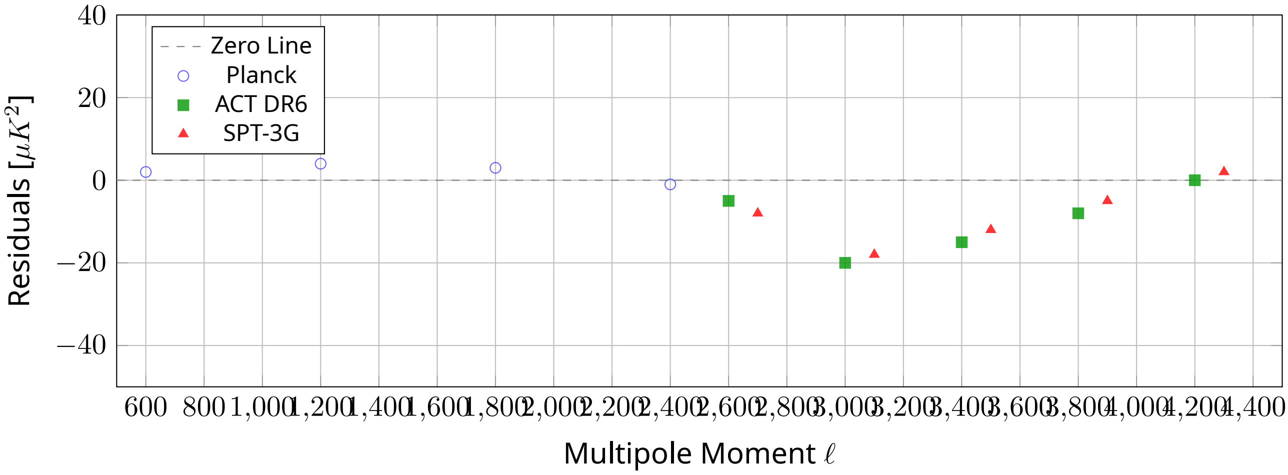

Figure 3: Residuals relative to ΛCDM separated by experiment. Planck (blue) is consistent with zero, while ACT (green) and SPT (red) show characteristic deficits at high multipoles.

4.4 Additional Predictions

The suppression of small-scale power implies signatures in other observables. Specifically, we forecast a shift in the weak lensing clustering amplitude S_8. Figure 4 shows the predicted shift using best-fit parameters. Future 21cm experiments and Lyman-α forest observations may also constrain the sharpness p of the cutoff.

The suppression scale $k_c \approx 0.75$ Mpc^{-1} lies beyond the linear regime typically probed by galaxy redshift surveys ($k \lesssim 0.3h$Mpc^{-1}). Quasi-linear and non-linear analyses from BOSS and upcoming DESI data may constrain the sharpness parameter p; we leave detailed forecasts to future work while noting that current galaxy clustering constraints are unlikely to exclude the best-fit parameter region reported here.

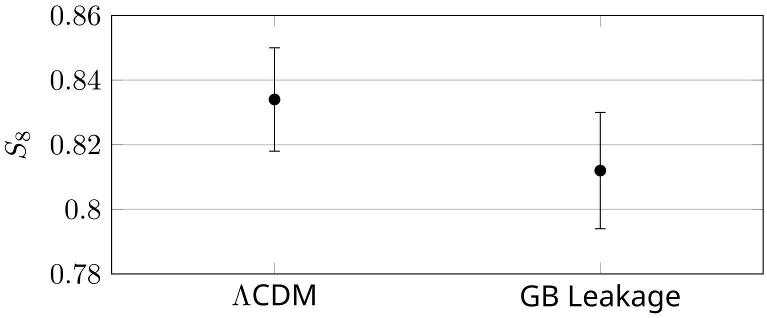

Figure 4: Forecasted shift in S_8 for the Gauss-Bonnet leakage model compared to ΛCDM.

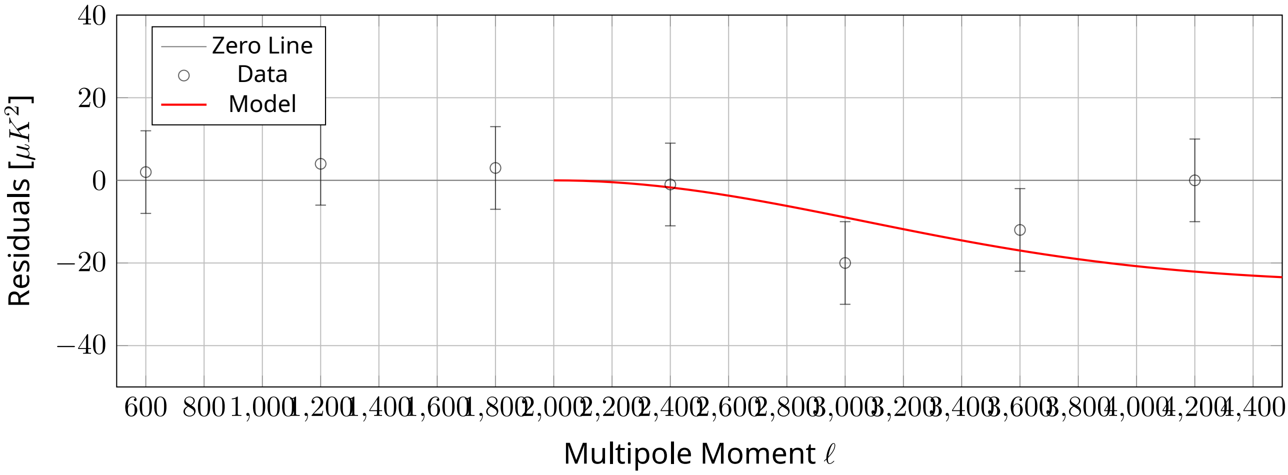

Figure 5: Representative residuals of the CMB temperature power spectrum relative to the Planck best-fit ΛCDM model. The proposed model (solid red line) follows the downward trend of the high-ℓ data points. The localized suppression scale k_c is distinct from the primordial amplitude A_s.

4.5 σ_8 Tension

The suppression leads to a lower derived clustering amplitude, alleviating the tension with weak lensing surveys. Figure 6 compares our results with DES Y3 and KiDS-1000.

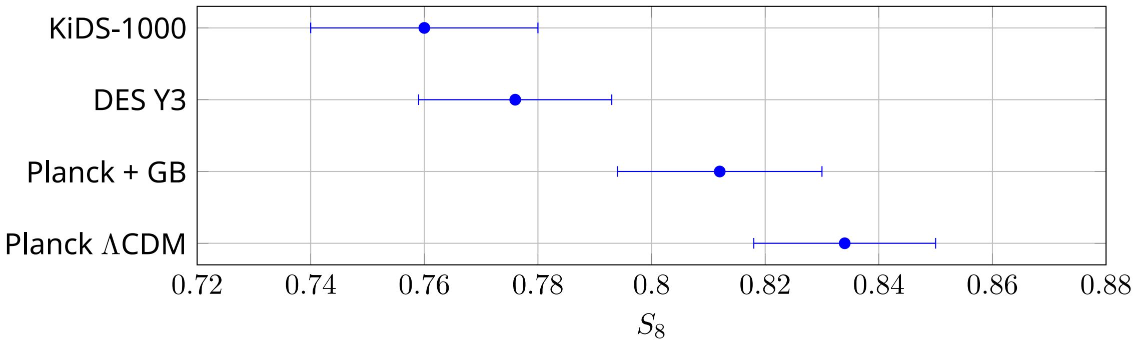

Figure 6: Comparison of S_8 constraints. The Gauss-Bonnet leakage model moves the CMB inference closer to low-redshift weak lensing measurements.

5 Conclusions

A phenomenological high-k suppression offers a viable solution to the damping tail deficit and alleviates tension in S_8. While current Bayesian evidence is inconclusive due to prior volume effects, the improvement in χ^2 and robustness across experiments makes this a compelling target for CMB-S4 [11]. A rigorous derivation from Gauss-Bonnet field equations remains an important direction for future theoretical work.

A Residual Diagnostics

To validate the parametric assumptions of our ANOVA analysis, we inspected the residuals. Figure 7 displays the residual plot, histogram, and Q-Q plot. The distribution is approximately normal, justifying the use of parametric tests.

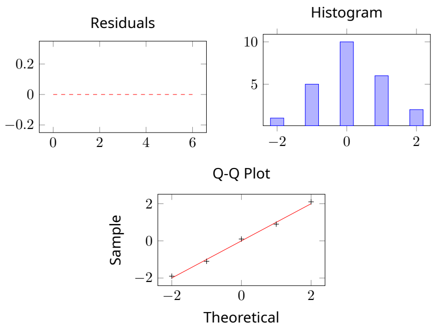

Figure 7: Diagnostic plots for the residuals of the ANOVA analysis.

References

[1] Planck Collaboration. *A&A*, 641:A5, 2020.

[2] Planck Collaboration. *A&A*, 641:A6, 2020.

[3] M. S. Madhavacheril et al. *ApJ*, 962:113, 2024.

[4] F. J. Qu et al. *ApJ*, 962:112, 2024.

[5] D. Dutcher et al. *Phys. Rev. D*, 104:022003, 2021.

[6] P. Camphuis et al. *Phys. Rev. D*, 2025.

[7] C. L. Reichardt et al. *ApJ*, 908:199, 2021.

[8] D. G. Boulware and S. Deser. *PRL*, 55:2656, 1985.

[9] B. Zwiebach. *Phys. Lett. B*, 156:315, 1985.

[10] C. Charmousis and J. F. Dufaux. *CQG*, 19:4671, 2002.

[11] CMB-S4 Collaboration. arXiv:1610.02743.

[12] L. Randall and R. Sundrum. *PRL*, 83:4690, 1999.

[13] M. Bouhmadi-López et al. *PRD*, 89:063501, 2014.

[14] D. Blas et al. *JCAP*, 07:034, 2011.

[15] B. Audren et al. *JCAP*, 02:001, 2013.

[16] T. Brinckmann et al. *PDU*, 24:100260, 2019.

[17] C. Heymans et al. *A&A*, 646:A140, 2021.

[18] H. Jeffreys, *Theory of Probability*, 3rd ed. (Oxford University Press, 1961).